COMPARISON STUDY OF PHOTOCATALYTIC DEGRADATION OF METHYLENE BLUE AND RHODAMINE B WITH ZnO NANORODS PREPARED BY USING THE HYDROTHERMAL METHOD

Pham Van Tuan[1*], Hoang Phi Hung[1], Nguyen Ngoc Vu[1], Le Tien Ha[2], Tran Thi Quynh Hoa[3], Vu Thi Tan[4], Tran Ngoc Khiem[1]

[1]*School of Materials Science and Engineering - Hanoi University of Science and Technology*
[2]*TNU - University of Science,* [3]*Hanoi University of Civil Engineering (HUCE)*
[4] *School of Chemistry and Life Sciences - Hanoi University of Science and Technology*

ARTICLE INFO

Received: 26/4/2024
Revised: 31/5/2024
Published: 31/5/2024

KEYWORDS

ZnO nanorods
Hydrothermal temperature
Photocatalytic activity
Methylene Blue
Decomposition of Rhodamine B

ABSTRACT

In this study, ZnO nanorods were fabricated by hydrothermal method at temperatures of 100, 120, 140 and 160 ^{o}C. ZnO nanorods have diameters from 50 nm to 100 nm and lengths up to several μm with the typical hexagonal structure of ZnO material with (100), (002), (101), (102), (110), (103), (200), (112), (004), (201), and (202) lattice planes. The positions of the peaks are almost unchanged with different hydrothermal temperatures. The Raman scattering analysis shown characteristic vibration modes of ZnO material at 100 cm^{-1}, 200 cm^{-1}, 331 cm^{-1}, 378 cm^{-1} and 436 cm^{-1} related to A_1, E_2 energy levels. UV-vis results show that the material absorbs strongly in the near ultraviolet band at 374 nm and gives characteristic emission of ZnO at 401 and 455 nm. The decomposition process of Methylene blue (MB) and Rhodamine B (RhB) for ZnO nanorod samples was studied under the visible light. The results shown that the synthesized ZnO material has the ability to decompose MB up to 94.96% and RhB up to 17.82 % after 120 minutes of illumination.

NGHIÊN CỨU SO SÁNH QUÁ TRÌNH PHÂN HỦY QUANG XÚC TÁC XANH METHYLENE VÀ RHODAMINE B VỚI THANH NANO ZnO CHẾ TẠO BẰNG PHƯƠNG PHÁP THỦY NHIỆT

Phạm Văn Tuấn[1*], Hoàng Phi Hùng[1], Nguyễn Ngọc Vũ[1], Lê Tiến Hà[2], Trần Thị Quỳnh Hoa[3], Vũ Thị Tần[4], Trần Ngọc Khiêm[1]

[1]*Trường Vật liệu - Đại học Bách khoa Hà Nội,* [2]*Trường Đại học Khoa học - ĐH Thái Nguyên*
[3]*Trường Đại học Xây dựng,* [4] *Trường Hóa và Khoa học Sự sống - Đại học Bách khoa Hà Nội*

THÔNG TIN BÀI BÁO

Ngày nhận bài: 26/4/2024
Ngày hoàn thiện: 31/5/2024
Ngày đăng: 31/5/2024

TỪ KHÓA

Thanh nano ZnO
Phương pháp thủy nhiệt
Quang xúc tác
Xanh Methylene
Phân hủy Rhodamine B

TÓM TẮT

Trong nghiên cứu này, thanh nano ZnO được chế tạo bằng phương pháp thủy nhiệt ở nhiệt độ 100, 120, 140 và 160 ^{o}C. Các thanh nano ZnO có đường kính từ 50 nm đến 100 nm và có chiều dài lên tới vài μm với cấu trúc lục giác đặc trưng của vật liệu ZnO với các mặt phẳng (100), (002), (101), (102), (110), (103), (200), (112), (004), (201), và (202). Vị trí của các đỉnh hầu như không thay đổi ở các nhiệt độ thủy nhiệt khác nhau. Phân tích tán xạ Raman cho thấy các dạng dao động đặc trưng của vật liệu ZnO ở 100 cm^{-1}, 200 cm^{-1}, 331 cm^{-1}, 378 cm^{-1} và 436 cm^{-1} liên quan đến các mức năng lượng A_1, E_2. Kết quả UV-vis cho thấy vật liệu hấp thụ mạnh ở vùng tử ngoại gần ở bước sóng 374 nm và cho phát xạ đặc trưng của ZnO ở bước sóng 401 và 455 nm. Quá trình phân hủy xanh Methylene (MB) và Rhodamine B (RhB) đối với các mẫu thanh nano ZnO được nghiên cứu dưới ánh sáng khả kiến. Kết quả cho thấy, vật liệu thanh nano ZnO có khả năng phân hủy MB lên tới 94,96% và RhB lên tới 17,82% sau 120 phút chiếu sáng.

DOI: https://doi.org/10.34238/tnu-jst.10226

[*] Corresponding author. *Email: tuan.phamvan@hust.edu.vn*

1. Introduction

In recent years, the use of various dyes in industries such as textile, leather, paper, and other fields has increased significantly. However, polluted water from industries containing dyes has significantly affected biological life and human water sources due to their toxicity and persistent decomposition. Metal oxide semiconductors such as TiO_2, ZnO, and SnO_2 are used as effective photocatalysts for environmental degradation reactions [1] – [4]. Their unique properties such as high electron mobility, fast charge transfer, tunable band gap, stability, low cost, and environmental friendliness make them candidates for use as photocatalysts in environmental applications [2] – [7].

ZnO is the most common n-type semiconductor material, with unique physical and chemical properties [8] – [12]. Thus, ZnO is a promising material for various applications such as photocatalysis, solar cells, sensors, and optoelectronics. In the field of photocatalysis, the surface area of the material is important to increase the adsorption rate of dye molecules, absorbing incident light for the purpose of decomposing dye molecules [4], [5], [11] – [14]. In semiconducting metal oxides, ZnO exhibits enhanced photocatalytic activity through the generation of oxygen vacancies on the surface [4]. Oxygen vacancies serve as active sites for adsorption of contaminants and facilitate photocatalysis by acting as charge transfer gates between ZnO nanomaterials and molecules adsorbed [4]. Creating oxygen vacancies on the ZnO surface can improve the photocatalytic performance of the material considerably, leading to better environmental remediation results [4]. In addition, the photocatalytic process of ZnO depends on the properties of the material such as crystallite size, shape as well as synthesizing conditions of materials [8], [9], [15], [16].

In recent years, several new methods have been developed to control ZnO nanostructures and morphology [6], [7], [11], [17] – [21]. ZnO with many different morphologies such as nanowires, nanosheets, nanorods, nanotubes, nanonails, nanospheres, nanoneedles, nanopins, nanoflowers, nanobelts, and nanopencils are prepared by different methods such as vapor phase, wet chemistry, and chemical reactions [6], [7], [17] – [21]. Nowadays, photocatalytic performance is tuned and enhanced by creating desirable physicochemical properties related to size, and morphology [5], [14], [15]. Targeting the degradation of environmental pollutants depends on the specific crystal face expression of nanomaterials. Therefore, crystalline surface engineering is a very importance strategy. However, controlling the aspect of ZnO photocatalysts remains a challenge, from which their photocatalytic activity and industrial applications are limited.

In this study, we report on the hydrothermal synthesis of ZnO nanorods and the change in photocatalytic properties with different hydrothermal temperatures in the decomposition of Methylene blue (MB) and Rhodamine B (RhB) under visible light. Firstly, the influence of hydrothermal temperature on the crystal structure, material morphology, and optical properties of the material is studied. Then, the photocatalytic properties of ZnO nanorods in the degradation of MB and RhB were compared. Furthermore, the relationship between the structural, morphology, optical, and photocatalytic properties of ZnO nanorods was discussed.

2. Experiment

2.1. Materials

Zinc acetate dihydrate ($Zn(CH_3COO)_2.2H_2O$), potassium hydroxide (KOH), methanol (CH_3OH), and MB ($C_{16}H_{18}C_lN_3S$) were purchased from Sigma-Aldrich. All other chemicals were of analytical grade and used as received without purification.

2.2. Synthesis of ZnO nanorods

First, 10 g of $Zn(CH_3COO)_2.2H_2O$ in 70 ml of methanol were dissolved with a magnetic stirrer at room temperature for 30 minutes to obtain solution A. Next, 5 g of KOH were dissolved

in 50 ml of methanol with a magnetic stirrer at room temperature for 30 minutes to obtain solution B. Solution B was then dropped slowly into solution A, and the mixture was stirred slowly at room temperature for 30 minutes. Then, this solution mixture was placed in a water bath at a temperature of 100 °C, and stirring was continued for 25 minutes to form a homogeneous solution. The resulting mixture was poured into a Teflon autoclave and hydrothermally heated at a temperature of 100 ℃ for 24 h. After the hydrothermal process, the hydrothermal autoclave was naturally cooled to room temperature. The resulting precipitate was filtered and washed with a centrifuge at a speed of 4000 rpm and every 5 minutes with distilled water and methanol to remove excess ions remaining in the sample. Finally, the precipitate was dried at 80 ℃ for 24 h. The final product obtained is white ZnO powder. ZnO samples with hydrothermal temperatures of 120 °C, 140 °C, and 160 °C were fabricated through a similar process. These samples are named ZnO-100 °C, ZnO-120 °C, ZnO-140 °C, and ZnO-160 °C corresponding to hydrothermal temperatures of 100 °C, 120 °C, 140 °C, and 160 °C.

2.3. Characterization techniques

An X-ray diffractometer with Cu-Kα radiation at wavelength λ = 1.5406 Å was used to study the crystal structure and size of the ZnO material. A UV-visible spectrophotometer (V-650 Jasco, USA) was used to measure the UV-vis absorption spectra of the ZnO material. A field emission scanning electron microscope (FESEM; Hitachi S-4800) was used to study the surface morphology and size of the ZnO nanorods. The photoluminescence properties of materials used studied by photoluminescence spectroscopy at an excitation wavelength of 370 nm using a 250 W Xe lamp and the structural properties and vibration modes of ZnO samples was investigated by Raman scattering spectra.

2.4. Photocatalytic degradation experiments

MB and RhB dyes were used as contaminants to evaluate the photocatalytic performance of ZnO nanorod samples. In this experiment, 0.01 g of catalyst was dissolved into 100 mL of dye solution in a photocatalytic reactor to decompose MB and RhB. The catalyst and dye solution were stirred magnetically for 30 minutes in the dark. Then, the solution mixture was illuminated with visible light. Every 20 minutes of illumination, 5 mL of the mixture were taken out and centrifuged to remove the catalyst and measure the absorption spectra of the remaining solution to investigate the photocatalytic decomposition of the dye. The photocatalytic degradation efficiency of ZnO nanorod material is determined in % using the following formula [21]–[23]:

$$\%D = \frac{C_0 - C_t}{C_0} \times 100 \quad (1)$$

where C_0 and C_t are the absorbance of the dye before illumination and at different illumination durations, respectively.

3. Results and Discussion

X-ray diffraction pattern is used to determine the crystal phase, structure, and purity of ZnO nanomaterials. Figure 1 shows the X-ray diffraction patterns of ZnO nanorods with different hydrothermal temperatures. The results show that the diffraction peaks are intense and sharp, indicating a high degree of crystallinity of the ZnO nanomaterial. The diffraction peak positions of the ZnO samples were observed at 31.62°, 34.27°, 36.06°, 47.35°, 56.32°, 62.65°, 66.16°, 67.77°, 68.88°, 72.31°, and 76.84°, corresponding to the (100), (002), (101), (102), (110), (103), (200), (112), (004), (201), and (202) crystal planes of ZnO [20], [21], [23], [24]. The positions of these diffraction peaks are consistent with the JCPDS standard card (PDF card no. 04-003-2106) for the hexagonal structure of the ZnO crystal lattice [21]. When the hydrothermal temperature is changed, the position of the diffraction peaks does not change. This finding proves that

hydrothermal temperature does not affect the diffraction peak position of ZnO. However, with different hydrothermal temperatures of 100 °C, 120 °C, and 160 °C, the diffraction peak (101) has greater intensity than the diffraction peak (100). This condition proves that ZnO nanorods grow mainly in the (101) direction. However, when ZnO nanorods are fabricated with a hydrothermal temperature of 140 °C, the (100) diffraction peak surprisingly has a greater intensity than the (101) diffraction peak, thus demonstrating that the ZnO nanorods grow mainly in the (100) direction. The (100) peak has a higher intensity than the (101) peak, which is explained by the fact that 140 °C is the appropriate temperature to grow ZnO nanocrystals in the (100) direction compared to the (101) direction. This result is interesting, indicating that changing the hydrothermal temperature enables the growth direction of ZnO nanorods to be controlled.

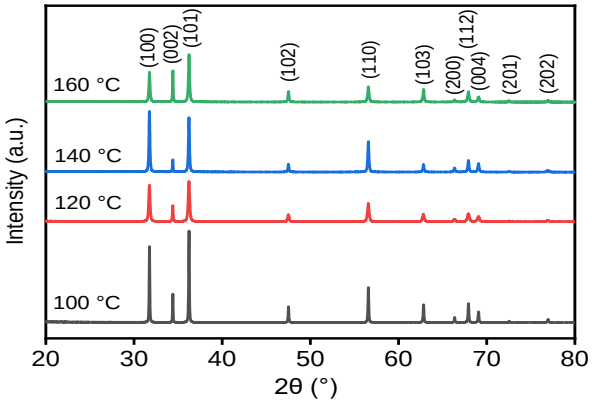

Figure 1. *X-ray diffraction patterns of ZnO nanorods at different hydrothermal temperatures*

From the results of X-ray diffraction measurements, we can determine the crystallite size of ZnO nanorods using the Debye–Scherrer expression [24]–[26].

$$D = 0.9\lambda/(\beta \cos\theta) \quad (2)$$

where D is the average crystallite size, λ is the wavelength of the X-ray (1.5406 Å), θ is half the Bragg diffraction angle, and β stands for FWHM. In addition, the interplane distance (d), lattice constants a and c of ZnO are determined by formulas (3) and (4) [27], [28].

$$n\lambda = 2d\ sin\ \theta \quad (3)$$

$$\frac{1}{d^2} = \frac{4}{3}\left(\frac{h^2 + hk + k^2}{a^2}\right) + \frac{l^2}{c^2} \quad (4)$$

where h, k, and l are Miller indices; a and c are lattice constants; and d is the interplane distance. The average crystal size, the interplane distance, and lattice constants are presented in Table 1.

Figure 2 presents FESEM images of ZnO samples fabricated at different hydrothermal temperatures: (A_1–A_2) 100 °C, (B_1–B_2) 120 °C, (C_1–C_2) 140 °C, and (D_1–D_2) 160 °C. The results show that the ZnO nanorods formed in Figures A_1–A_2 grow uniformly. Individual nanorods are about 100 nm to 200 nm wide and about 1 μm to 2 μm long. Evidently, the ZnO nanorods exhibit a distinct hexagonal structure. When the hydrothermal temperature increases to 120 °C in Figures B_1–B_2, the width of the ZnO nanorods is about 50 nm to 70 nm, and the length of the ZnO nanorods is about 2 μm to 3 μm. Compared with the hydrothermal sample at 100 °C, the width of the ZnO nanorods decreased significantly and the length of the ZnO nanorods increased. This condition can be explained by the fact that at high hydrothermal temperature and pressure, ZnO crystal seeds grow faster, causing the width of the ZnO nanorod to decrease and the length of the ZnO nanorod to increase. When the hydrothermal temperature continues to increase to 140 °C (Figures C_1–C_2) and 160 °C (Figures D_1–D_2), the width of the ZnO nanorod and the length of the ZnO nanorod are similar to those of the hydrothermal sample at 120 °C. From this observation, we can control the width and length of ZnO nanorods by using the hydrothermal temperature. This result is interesting for the study of photocatalytic properties. In comparison with the crystal

size results calculated from XRD shows that the crystallite sizes calculated from XRD are generally smaller than those observed from FESEM images. This result is explained as follows: Crystallite crystal size is calculated from XRD. These are homogeneous crystalline regions (coherent scattering regions). The ideal crystal is an infinite homogeneous region where XRD only obtains peaks that are lines. But in reality, the region where the crystals are periodically arranged uniformly is only small, so the XRD peak is broadened. The smaller the homogeneous area, the wider the peak. When observing nanorods from FESEM images, these nanorods contain several different uniform crystalline regions, so the crystallite size is smaller than the size observed from FESEM. If the nanoparticles are small, each nanoparticle is a uniform region, then the crystallite size is equal to the particle size.

Table 1. *Average crystallite size, lattice constants, and d-spacing of ZnO nanorods at different hydrothermal temperatures*

Sample	Position (2θ)	(hkl)	FWHM	Crystallite size (D) (nm)	Average crystallite size (nm)	d-spacing (nm)	Lattice parameters a = b (nm)	Lattice parameters c (nm)
ZnO-100 °C	31.75	(100)	0.09	95.89	97.28	0.26	0.30	0.52
	34.40	(002)	0.08	108.62				
	36.24	(101)	0.10	87.34				
ZnO-120 °C	31.74	(100)	0.20	43.15	54.58	0.26	0.30	0.52
	34.40	(002)	0.11	78.99				
	36.23	(101)	0.21	41.59				
ZnO-140 °C	31.75	(100)	0.15	57.53	66.34	0.26	0.30	0.52
	34.40	(002)	0.10	86.89				
	36.23	(101)	0.16	54.59				
ZnO-160 °C	31.75	(100)	0.17	50.76	66.23	0.26	0.30	0.52
	34.40	(002)	0.09	96.55				
	36.24	(101)	0.17	51.38				

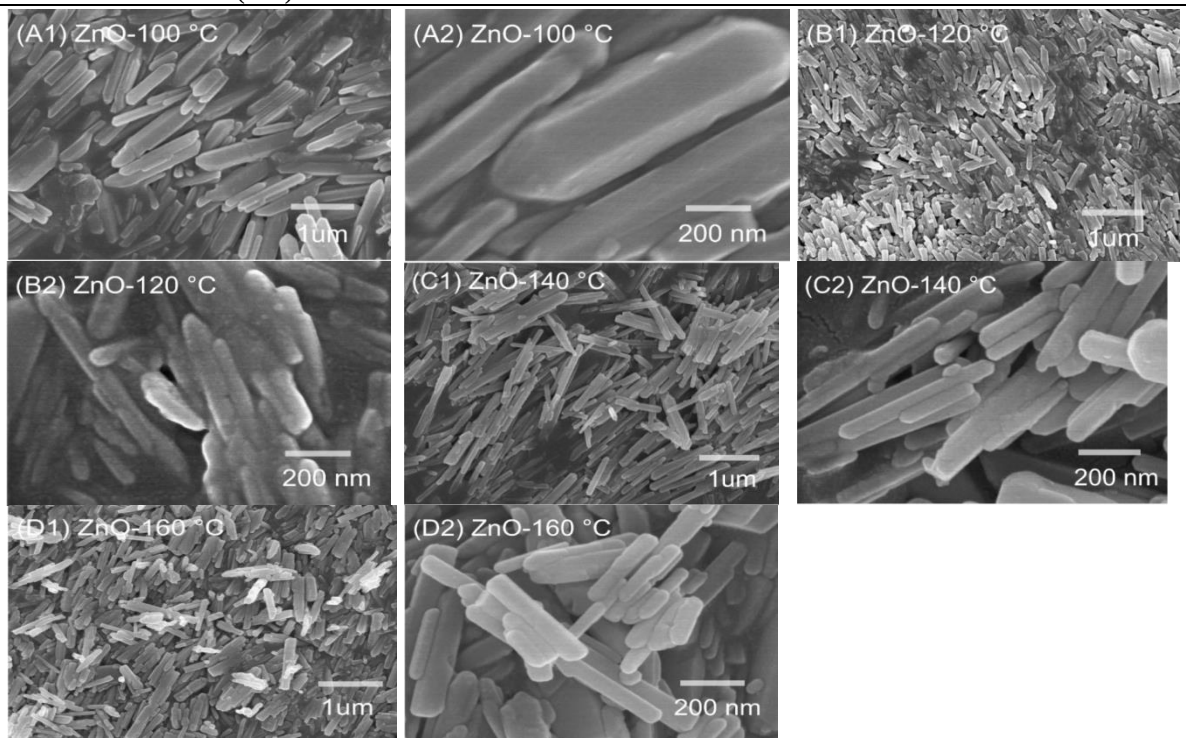

Figure 2. *FESEM images of ZnO nanorods at different hydrothermal temperatures*

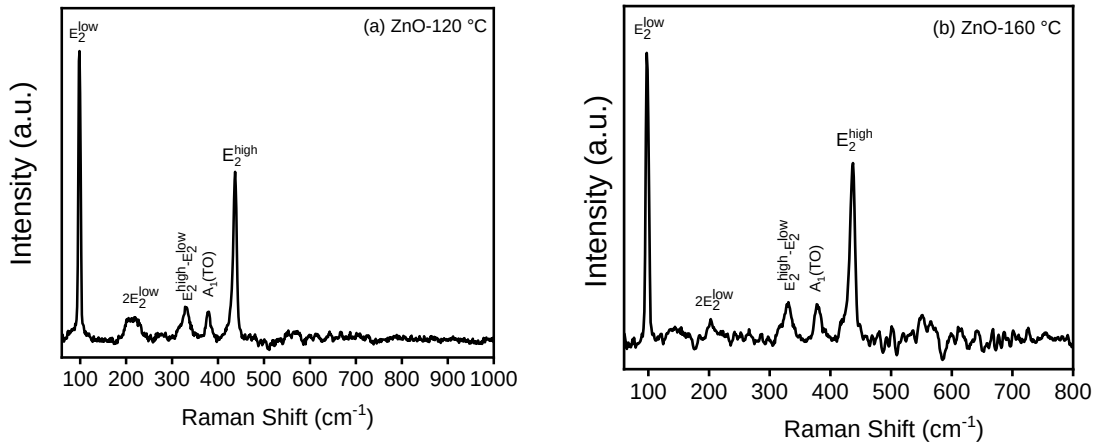

Figure 3. *Raman spectra of ZnO nanorods: (a) ZnO-120 °C, (b) ZnO-160 °C*

Raman spectroscopy was used to study the presence and absence of vibrational modes in ZnO nanorod samples [29]. Figure 3 shows the Raman scattering spectra of ZnO-120 °C, ZnO-160 °C samples. The main Raman vibrational modes of the wurtzite structure of ZnO were found for ZnO samples. This result is consistent with the X-ray diffraction results. For ZnO nanorod samples, the most intense Raman peaks is located at 100 cm^{-1} and 436 cm^{-1} corresponding to the E_2^{low} and E_2^{high} Raman modes [28], [29]. Other Raman peaks were observed at 200 cm^{-1}, 331 cm^{-1}, and 378 cm^{-1} corresponding to the $2E_2^{low}$, $E_2^{high} - E_2^{low}$, $A_1(\mathrm{TO})$ modes [28], [29]. E_2 modes are unpolarized and do not exhibit LO and TO splitting [29]. E_2 mode is divided into E_2^{high} and E_2^{low} due to its frequency at point Γ in the Brillouin zone [29].

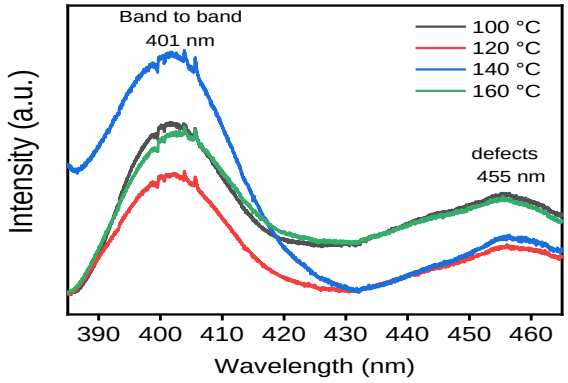

Figure 4. *PL spectra of ZnO nanorods at different hydrothermal temperatures*

The photoluminescence spectra of ZnO nanorods are plotted in Figure 4. The photoluminescence spectra were measured at room temperature with an excitation wavelength of 370 nm. The photoluminescence spectra of ZnO nanorod samples include two emission bands: near-band edge (NBE) emission at a wavelength of 401 nm and visible emission band at a wavelength of 455 nm. The NBE emission is related to the band-to-band recombination of ZnO nanocrystals [16], [23] – [25], [30], [31]. The shift of the diffraction peak of nanorods can be related to the morphology and size of the ZnO nanostructures [16], [23]–[25], [30]. The visible emission band is due to intrinsic defects such as zinc vacancies and the combination of zinc vacancies and zinc interstitials [16], [23] – [25].

UV-vis absorption spectroscopy was performed to study the absorption properties of ZnO nanorod samples. The characteristic ZnO peaks of the ZnO nanorod samples were observed in the range of 350–400 nm [8], [20], [24], [32]. As observed in Figure 5, the values of UV peaks

are 377, 376, 376, and 374 nm, which correspond to the samples ZnO-100 °C, ZnO-120 °C, ZnO-140 °C, and ZnO-160 °C. The position of the UV-vis absorption peak of the samples did not change much. However, the intensity of the UV-vis absorption peak of the ZnO nanorod samples increased significantly when the hydrothermal temperature increased from 100 °C to 160 °C. This condition is explained by the increased crystallinity of the sample, causing the absorption intensity to increase.

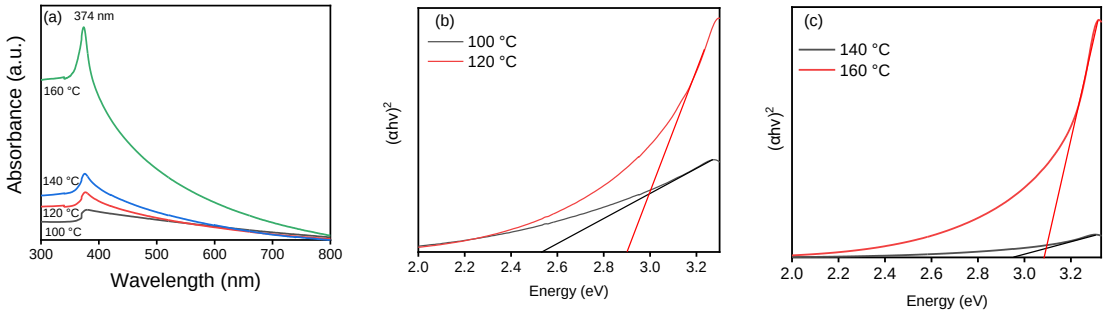

Figure 5. *(a) UV-vis absorption spectra and (b, c) Tauc plots of ZnO nanorods at different hydrothermal temperatures*

Formula (5) is used to calculate the band gap value of ZnO nanorod samples [8], [20], [32], where α indicates the absorption coefficient, E_g is the band gap, hν represents the photon energy, and A is a constant. As shown in Figs. 5b and 5c, $(\alpha h\nu)^2$ versus (hν) is plotted to calculate the band gap energy. The band gap of the samples ZnO-100 °C, ZnO-120 °C, ZnO-140 °C, and ZnO-160 °C is calculated as 2.53, 2.90, 2.96, and 3.09 eV, respectively. This result shows that when the hydrothermal temperature increases from 100 °C to 160 °C, the band gap increases from 2.53 eV to 3.09 eV. This condition can be explained by the decrease in nanorod width as the hydrothermal temperature increases.

$$\alpha(h\nu) = A(h\nu - E_g)^{1/2} \quad (5)$$

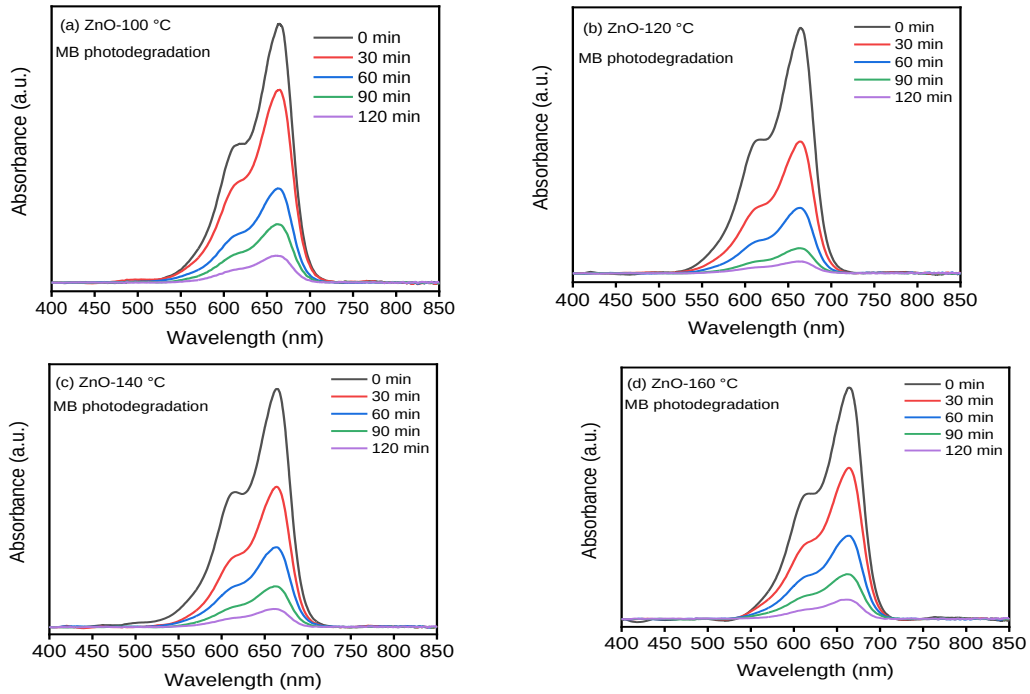

Figure 6. *UV-vis absorption spectra of MB dye solution containing ZnO nanorods during illumination: (a) ZnO-100 °C, (b) ZnO-120 °C, (c) ZnO-140 °C, and (d) ZnO-160 °C*

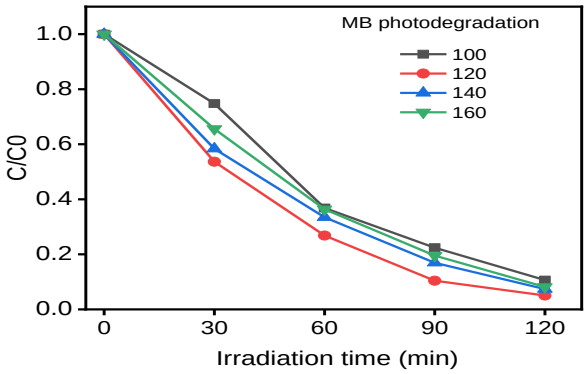

Figure 7. *Photocatalytic performance of MB degradation with ZnO-100 °C, ZnO-120 °C, ZnO-140 °C, and ZnO-160 °C nanorods*

The photocatalytic properties of ZnO nanorods were studied by MB decomposition. Figure 6 shows the absorption spectra of MB solution containing nanorods according to illumination time. The lighting time surveyed was from 0 to 120 minutes. The results show an absorption peak at 655 nm and an absorption shoulder at 630 nm, which are the characteristic absorption peaks of the MB solution [8], [21], [23], [27]. When the illumination time increases from 0 min to 120 min, the position of the MB absorption peaks does not change, while the MB absorption intensity decreases sharply.

To study the photocatalytic performance of ZnO nanorods over time, we analyzed the change in C/C_0 concentration ratio with illumination time. Figure 7 shows the photocatalytic degradation performance of ZnO nanorod samples with different hydrothermal times for MB dye. The results showed that the MB photodegradation efficiency of these samples ranged from 89.36%, 94.96%, 92.61% and 91.85% with ZnO-100 °C, ZnO-120 °C, ZnO-140 °C, and ZnO-160 °C samples. Photocatalytic performance depends on crystal size and surface area. As the crystallite size is calculated from XRD and observed nanorod size from FESEM images, we see that the ZnO-100 °C sample has the largest size and therefore the smallest surface area. Therefore, the photocatalytic degradation efficiency is smaller than the ZnO-120 °C, ZnO-140 °C, and ZnO-160 °C samples. Meanwhile, ZnO nanorods from the ZnO-120 °C, ZnO-140 °C, and ZnO-160 °C samples have similar crystallite size and morphology, so the photocatalytic degradation efficiency of the samples works similar.

Research on the photocatalytic properties of ZnO nanorods was also conducted by decomposing RhB solution containing ZnO nanorods under the influence of light. Figure 8 shows the absorption spectra of RhB containing ZnO nanorod samples with different illumination times. The lighting time surveyed was from 0 minutes to 120 minutes. The results showed that a characteristic absorption peak of RhB was observed at 550 nm in all samples [2], [7], [17], [33]. As the illumination time increased, the RhB absorption peak intensity decreased slightly in all samples.

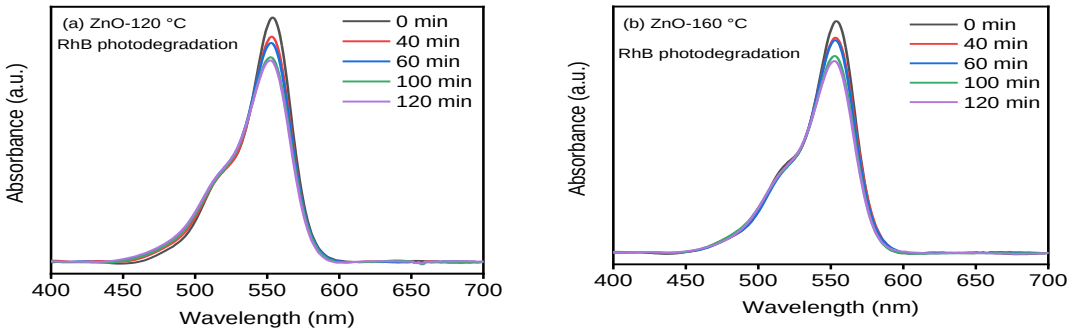

Figure 8. *Time-dependent photodegradation absorption spectra of RhB dye in the presence of ZnO nanorods during illumination: (a) ZnO-120 °C, (b) ZnO-160 °C*

To study the change in RhB absorption intensity according to illumination time, we plot the change in C/C_0 of RhB solution with different samples (where C is the RhB absorption concentration at time t, and C_0 is the absorption concentration of RhB before illumination). Figure 9 shows the photocatalytic performance of RhB degradation with ZnO-120 °C, ZnO-160 °C. For ZnO nanorod samples with different hydrothermal temperatures, the decomposition efficiency ranged from 17.82% to 17.25% with ZnO-120 °C, ZnO-160 °C.

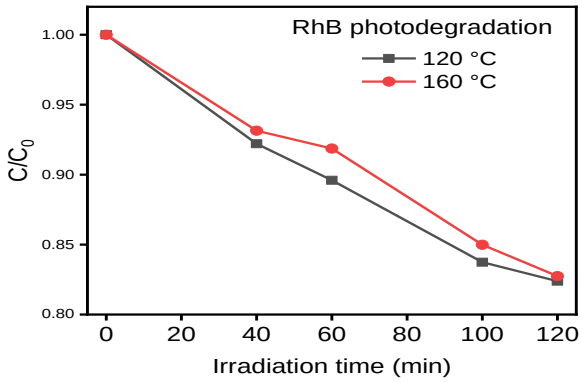

Figure 9. *Photocatalytic performance of RhB degradation with ZnO-120 °C, ZnO-160 °C*

A comparison of the photocatalytic degradation performance of ZnO nanorod samples in the degradation of MB and RhB shows that the ZnO nanorods photodegrades MB better than they photodegrades RhB. The photocatalytic degradation efficiency of ZnO nanorods for MB is about over 90%, while that for RhB is only about 18%. Previous results of photocatalytic research on MB and RhB show that the degradation efficiency of MB is always higher than that of RhB [34–38]. This is explained by the different nature of the chemical bonds and composition in MB and RhB molecules. Chemical structure of Rhodamine B includes four benzene rings, while chemical structure of Methylene Blue includes three benzene rings [38]. RhB includes three interconnected rings and one separate ring [38], so RhB has high stability.Therefore, RhB is more difficult to degrade than MB.

4. Conclusions

We successfully fabricated ZnO nanorods by using the hydrothermal method at hydrothermal temperatures from 100 °C to 160 °C. ZnO nanorods have a width of about 50 nm to 70 nm and a length of about 2 to 3 μm. As the hydrothermal temperature increases, the width of the ZnO nanorods decreases and the length of the nanorods increases. Studying the X-ray diffraction of the samples shows that the ZnO nanorods mainly grew in the (101) direction. The Raman scattering spectrum of ZnO nanorods shows that the characteristic peaks of ZnO are clearly evident, with the most intense Raman peaks is located at 100 cm^{-1} and 436 cm^{-1} corresponding to the E_2^{low} and E_2^{high} Raman modes, and other Raman peaks were observed at 200 cm^{-1}, 331 cm^{-1}, and 378 cm^{-1} corresponding to the $2E_2^{low}$, $E_2^{high} - E_2^{low}$, $A_1(\mathrm{TO})$ modes. The photoluminescence spectra of the ZnO nanorod samples show two emission bands at 401 nm corresponding band to band emission and at 455 nm corresponding to the defects. The absorption spectra of ZnO nanorods shows a characteristic absorption peak of ZnO at 376 nm corresponding to the band absorption of ZnO. The MB photodegradation efficiency of these samples ranged from 89.36%, 94.96%, 92.61% and 91.85% with ZnO-100 °C, ZnO-120 °C, ZnO-140 °C, and ZnO-160 °C samples. A comparison of the photocatalytic degradation of RhB and MB indicates that the degradation of MB has a higher efficiency than the degradation of RhB with the same ZnO nanorod sample.

Acknowledgments

This research was funded by the Vietnam Ministry of Education and Training under project number B2023-BKA-01.

REFERENCES

[1] V. Kumar, R. Gupta, and A. Bansal, "Hydrothermal Growth of ZnO Nanorods for Use in Dye-Sensitized Solar Cells," *ACS Appl. Nano Mater.*, vol. 4, pp. 6212–6222, 2021.

[2] S. Shabna, S. S. J. Dhas, and C. S. Biju, "Potential progress in SnO2 nanostructures for enhancing photocatalytic degradation of organic pollutants," *Catal. Commun.*, vol. 177, 2023, Art. no. 106642.

[3] W. Vallejo, A. Cantillo, and C. Díaz-Uribe, "Improvement of the photocatalytic activity of ZnO thin films doped with manganese, *Heliyon*, vol. 9, 2023, Art. no. e20809.

[4] A. Ranjbari, J. Kim, J. Yu, J. Kim, M. Park, N. Kim, K. Demeestere, and P. M. Heynderickx, "Effect of oxygen vacancy modification of ZnO on photocatalytic degradation of methyl orange: A kinetic study," *Catal. Today*, vol. 427, 2024, Art. no. 114413.

[5] Z. Shaghaghi, S. Mollaei, A. R. Amani-Ghadim, and Z. Abedini, "Green synthesis of ZnO nanoparticles using the aqueous extract of Platanus orientalis: Structural characterization and photocatalytic activity," *Mater. Chem. Phys.*, vol. 305, 2023, Art. no. 127900.

[6] B. Boro, J. S. Boruah, C. Devi, Alemtoshi, B. Gogoi, P. Bharali, P. V. B. Reddy, D. Chowdhury, and P. Kalita, "A novel route to fabricate ZnO nanoparticles using Xanthium indicum ethanolic leaf extract: Green nanosynthesis perspective towards photocatalytic and biological applications," *J. Mol. Struct.*, vol. 1300, 2024, Art. no. 137227.

[7] F. M. Sanakousar, C. Vidyasagar, V. M. Jiménez-Pérez, and K. Prakash, "Recent progress on visible-light-driven metal and non-metal doped ZnO nanostructures for photocatalytic degradation of organic pollutants," *Mater. Sci. Semicond. Process.*, vol. 140, 2022, doi: 10.1016/j.mssp.2021.106390.

[8] S. Mirza, A. A. Hussaini, G. Öztürk, M. Turgut, T. Öztürk, O. Tugay, D. Ulukuş, and M. Yıldırım, "Photocatalytic and antibacterial activities of ZnO nanoparticles synthesized from Lupinus albus and Lupinus pilosus plant extracts via green synthesis approach," *Inorg. Chem. Commun.*, vol. 155, 2023, doi: 10.1016/j.inoche.2023.111124.

[9] D. A. Karajz and I. M. Szilágyi, "Review of photocatalytic ZnO nanomaterials made by atomic layer deposition," *Surfaces and Interfaces*, vol. 40, 2023, doi: 10.1016/j.surfin.2023.103094.

[10] L. Liang and X. Shi, "Electrochemical and photocatalytic properties of ZnO nanostructures deposited on nanoporous anodized aluminum oxide membrane and its application for degradation of reactive blue 19 in textile wastewater," *Int. J. Electrochem. Sci.*, vol. 18, 2023, Art. no. 100272.

[11] C. B. Ong, L. Y. Ng, and A. W. Mohammad, "A review of ZnO nanoparticles as solar photocatalysts: Synthesis, mechanisms and applications," *Renew. Sustain. Energy Rev.*, vol. 81, pp. 536–551, 2018.

[12] G. K. Weldegebrieal, "Synthesis method, antibacterial and photocatalytic activity of ZnO nanoparticles for azo dyes in wastewater treatment: A review," *Inorg. Chem. Commun.*, vol. 120, 2020, Art. no. 108140.

[13] G. Revathi and N. U. Sangari, "Morphology dependent photocatalytic efficiency of nano ZnO towards Azure A dye," *Open Ceram.*, vol. 16, 2023, Art. no. 100465.

[14] H. Wu, M. Liu, Y. Quan, X. Tian, C. Ren, and Z. Wang, "Enhanced photocatalytic activity of ZnO microflowers by a trace amount of Ti3C2 MXene," *Inorg. Chem. Commun.*, vol. 157, 2023, Art. no. 111322

[15] A. K. Mourya, R. P. Singh, T. Kumar, A. S. Talmale, G. S. Gaikwad, and A V. Wankhade, "Tuning the morphologies of ZnO for enhanced photocatalytic activity," *Inorg. Chem. Commun.*, vol. 154, 2023, Art. no. 110850.

[16] A. Esbergenova, M. Yusupov, M. Ghasemitarei, R. Jalolov, M. Hojamberdiev, and U. Shaislamov, "Understanding the effect of morphological change on photocatalytic activity of ZnO nanostructures and reaction mechanism by molecular dynamics," *Colloids Surfaces A Physicochem. Eng. Asp.*, vol. 677, 2023, Art. no. 132386.

[17] M. Xie, D. Zhang, Y. Wang, and Y. Zhao, "Facile fabrication of ZnO nanorods modified with RGO for enhanced photodecomposition of dyes," *Colloids Surfaces A Physicochem. Eng. Asp.*, vol. 603, 2020, Art. no. 125247.

[18] M. Faisal, A. A. Ismail, A. A. Ibrahim, H. Bouzid, and S.A. Al-sayari, "Highly efficient photocatalyst based on Ce doped ZnO nanorods : Controllable synthesis and enhanced photocatalytic activity," *Chem. Eng. J.* vol. 229, pp. 225–233, 2013.

[19] E. A. Daher, C. Boissière, C. L. Robert, and W. Hamd, "Investigating the impact of chemical structures on the photocatalytic degradation rates over ZnO nanorods: An oxidative pathways perspective," *Catal.*

Commun., vol. 185, 2023, Art. no. 106807.
[20] M. Shoeb, S. Ahmad, F. Mashkoor, M. N. Khan, I. Hasan, B. R. Singh, and C. Jeong, "Investigating the size-dependent structural, optical, dielectric, and photocatalytic properties of benign-synthesized ZnO nanoparticles," *J. Phys. Chem. Solids*, vol. 184, 2024, Art. no. 111707.
[21] A. S. Giasari, A. P. M. Muharam, A. Syampurwadi, Dedi, D. R. Eddy, and I, Primadona, "Morphological effect of one-dimensional ZnO nanostructures on the photocatalytic activity," *J. Phys. Chem. Solids*, vol. 176, 2023, Art. no. 111259.
[22] J. S. Packialakshmi, M. F. Albeshr, A. F. Alrefaei, F. Zhang, X. Liu, T. Selvankumar, and R. Mythili, "Development of ZnO/SnO2/rGO hybrid nanocomposites for effective photocatalytic degradation of toxic dye pollutants from aquatic ecosystems," *Environ. Res.*, vol. 225, 2023, Art. no. 115602.
[23] J. Paul and M. C. S. Kumar, "Enhanced photocatalytic activity of graphene oxide incorporated ZnO nanorods doped with post-transition metals," *Ceram. Int.*, vol. 50, pp. 9081–9088, 2024.
[24] A. Villegas-Fuentes, A. R.-D. L. Torre, A. R. Vilchis-Nestor, and P. A. Luque, "Improvement of the optical, photocatalytic and antibacterial properties of ZnO semiconductor nanoparticles using different pepper aqueous extracts," *Chemosphere*, vol. 339, 2023, Art. no. 139577.
[25] C. Rajkumar, K. S. Balamurugan, C. K. Pradhan, A. Arulraj, M. Kalaiselvan, D. S. Arokia, A. C. R. Babu, V. R. M. Reddy, W. K. Kim, and A. Khan, "Influence of Sn4+ substitution on the ZnO crystal structure and their enhanced fibre optic gas sensing and photocatalytic degradation performance," *Phys. B Condens. Matter*, vol. 667, 2023, Art. no. 415139.
[26] D. R. Vaddi, K. Vinukonda, R. K. Patnala, Y. Kanithi, T. R. Gurugubelli, J. Bae, R. Koutavarapu, D. Y. Lee, and J. Shim, "Effect of yttrium doping on the crystal structure, optical, and photocatalytic properties of hydrothermally synthesized ZnO nanorods," *Mater. Sci. Eng. B*, vol. 296, 2023, Art. no. 116664
[27] C. Mrabet, R. Jaballah, N. Mahdhi, A. Boukhachem, and M. Amlouk, "CuO-ZnO nanocomposites-based thin films: Characterization, physical properties and sunlight photocatalytic degradation of organic pollutants," *J. Alloys Compd.*, vol. 968, 2023, Art. no. 172252.
[28] I. G. F. D. Sá, F. P. Araújo, F. E. P. D. Santos, M. B. Furtini, E. C. D. Silva-Filho, L. C. Almeida, M. D. E. Forbes, Y. G. Dávila, R. R. P. Garcia, and J. A. Osajima, "Synthesis of ZnO co-doped with Er and Co: Effect of the dopants on the structural, optical properties and yellow eosin photocatalytic response," *Solid State Sci.*, vol. 147, 2024, Art. no. 107400.
[29] A. S. Soares, S. Castro-Lopes, M. Cabrera-Baez, R. Milani, E. Padrón-Hernández, B. V. Farias, J. M. Soares, S. S. Gusmão, B. C. Viana, Y. Guerra, C. S. Oliveira, and R. Peña-Garcia, "The role of pH on the vibrational, optical and electronic properties of the Zn1-xFexO compound synthesized via sol gel method," *Solid State Sci.*, vol. 128, 2022, doi: 10.1016/j.solidstatesciences.2022.106880.
[30] A. Samal, K. Pouthika, A. Rajesh, S. M. Roopan, and G. Madhumitha, "Photocatalytic degradation and kinetic investigations of ZnO-SnO_2 heterostructures for treatment of methyl violet using non-conventional approach," *Inorg. Chem. Commun.*, vol. 159, 2024, Art. no. 111809.
[31] Q. Shi, Z. Luo, L. Jiang, X. Li, C. Bai, and Q. Yu, "Fabrication and photocatalytic properties of Co doped ZnO nanomaterials," *Mater. Lett.*, vol. 350, pp. 1–4, 2023.
[32] X. Zhang, L. Zhou, X. Tu, and F. Hu, "Hydrothermal synthesis of ZnO Crystals: Diverse morphologies and characterization of the photocatalytic properties," *Polyhedron*, vol. 246, 2023, Art. no. 116668.
[33] R. Firmansyah, R. Bakri, and Y. Yulizar, "Enhancement of photocatalytic activity of ZnO by ZnMoO4 compositing under visible light via hydrothermal green synthesis," *Inorg. Chem. Commun.*, vol. 155, 2023, Art. no. 110893.
[34] D. Neena, K. K. Kondamareddy, H. Bin, D. Lu, P. Kumar, R. K. Dwivedi, V. O. Pelenovich, X. Z. Zhao, W. Gao, and D. Fu, "Enhanced visible light photodegradation activity of RhB/MB from aqueous solution using nanosized novel Fe-Cd co-modified ZnO," *Sci. Rep.*, vol. 8, pp. 1–12, 2018.
[35] R. Jagadeeswari, G. Rathika, K. V. S. Kumar, and P. Selvakumar, "Surface parametric influences on the photocatalytic behaviour of zinc oxide nanoparticles," *J. Ovonic Res.*, vol. 20, pp. 115–124, 2024.
[36] S. Vishwanathan and S. Das, "Glucose-mediated one-pot hydrothermal synthesis of hollow magnesium oxide-zinc oxide (MgO-ZnO) microspheres with enhanced natural sunlight photocatalytic activity," *Environ. Sci. Pollut. Res.*, vol. 30, pp. 8512–8525, 2023.
[37] J. Gupta, J. Mohapatra, and D. Bahadur, "Visible light driven mesoporous Ag-embedded ZnO nanocomposites: reactive oxygen species enhanced photocatalysis, bacterial inhibition and photodynamic therapy," *Dalt. Trans.*, vol. 46, pp. 685–696, 2017.
[38] R. H. Waghchaure, V. A. Adole, and B. S. Jagdale, "Photocatalytic degradation of methylene blue, rhodamine B, methyl orange and Eriochrome black T dyes by modified ZnO nanocatalysts: A concise review," *Inorg. Chem. Commun.*, vol. 143, 2022, Art. no. 109764.